Journal of Materials Chemistry B



PAPER View Article Online



Cite this: DOI: 10.1039/d0tb00520g

Molecular simulations and understanding of antifouling zwitterionic polymer brushes†

Yonglan Liu,‡^a Dong Zhang,‡^a Baiping Ren,^a Xiong Gong, b Lijian Xu,^c Zhang-Qi Feng,^d Yung Chang, b Yi He f and Jie Zheng

Zwitterionic materials are an important class of antifouling biomaterials for various applications. Despite such desirable antifouling properties, molecular-level understanding of the structure-property relationship associated with surface chemistry/topology/hydration and antifouling performance still remains to be elucidated. In this work, we computationally studied the packing structure, surface hydration, and antifouling property of three zwitterionic polymer brushes of poly(carboxybetaine methacrylate) (pCBMA), poly(sulfobetaine methacrylate) (pSBMA), and poly((2-(methacryloyloxy)ethyl)phosporylcoline) (pMPC) brushes and a hydrophilic PEG brush using a combination of molecular mechanics (MM), Monte Carlo (MC), molecular dynamics (MD), and steered MD (SMD) simulations. We for the first time determined the optimal packing structures of all polymer brushes from a wide variety of unit cells and chain orientations in a complex energy landscape. Under the optimal packing structures, MD simulations were further conducted to study the structure, dynamics, and orientation of water molecules and protein adsorption on the four polymer brushes, while SMD simulations to study the surface resistance of the polymer brushes to a protein. The collective results consistently revealed that the three zwitterionic brushes exhibited stronger interactions with water molecules and higher surface resistance to a protein than the PEG brush. It was concluded that both the carbon space length between zwitterionic groups and the nature of the anionic groups have a distinct effect on the antifouling performance, leading to the following antifouling ranking of pCBMA > pMPC > pSBMA. This work hopefully provides some structural insights into the design of new antifouling materials beyond traditional PEG-based antifouling materials.

Received 26th February 2020, Accepted 15th March 2020

DOI: 10.1039/d0tb00520g

rsc.li/materials-b

1. Introduction

Zwitterionic polymers possess a unique structural feature, *i.e.*, a combination of an equal number of cationic groups (*e.g.* phosphonium, pyridinium, imidazolium and quaternary/tertiary/secondary/primary ammonium groups) and anionic groups (*e.g.* carboxylate, sulfonate and phosphate groups) in

the same pendant motif.^{1,2} Such a unique structural feature also endows zwitterionic polymers with different functional properties, including overall charge neutrality, high hydrophilicity, strong dipole pairs, and an anti-polyelectrolyte effect.3 Zwitterionic polymers can be fabricated into different structural forms of brushes, 4,5 hydrogels, 6-8 membranes, 9 films, 10 particles, 11 and coatings, 12 with different functions of antifouling, 7,8,12 stimuli-responsive, 13-16 antibacterial, 8 selfhealing,17 and lubrication18,19 properties for different applications of marine coatings, 12 wound dressings, 20 drug/gene delivery carriers, 21,22 biosensors, 23,24 and implants. Among these diverse structures, functions, and applications, zwitterionic polymers are still well recognized for their excellent antifouling property and used as antifouling coatings, comparable or even superior to poly(ethylene glycol) (PEG)-based coatings.²⁵⁻²⁷ The most common zwitterionic moieties include carboxybetaine (CB), sulfobetaine (SB), and phosphatidylcholine (PC), which are often used to be polymerized into polymer brushes via the grafting-to or grafting-from methods. The antifouling property of zwitterionic polymers is generally accepted to occur through the water barrier principle, where zwitterionic ion pairs strongly attract

^a Department of Chemical, Biomolecular, and Corrosion Engineering, The University of Akron, Ohio 44325, USA. E-mail: zhengj@uakron.edu

^b Department of Polymer Engineering, The University of Akron, Ohio 44325, USA

^c Hunan Key Laboratory of Biomedical Nanomaterials and Devices College of Life Science and Chemistry, Hunan University of Technology, Zhuzhou 412007, P. R. China

^d School of Chemical Engineering, Nanjing University of Science and Technology, Nanjing, 210094, China

^e Department of Chemical Engineering and R&D Center for Membrane Technology, Chung Yuan Christian University, Taoyuan 320, Taiwan

^f College of Chemical and Biological Engineering, Zhejiang University, Hangzhou, Zhejiang 310027, China

[†] Electronic supplementary information (ESI) available: Force field parameters for pCBMA, pSBMA, and pMPC. See DOI: 10.1039/d0tb00520g

[‡] These authors contributed equally to this work.

neighboring waters via electrostatically induced interactions to form a tightly and stably bound water layer on polymer brushes,²⁸ which would induce the formation of a physical and energy barrier to prevent the adsorption of proteins, cells, and bacteria, with the assistance of the steric repulsion of polymer chains.5,8,29-32

While experimental studies on zwitterionic brushes have been intensively conducted to demonstrate their surface resistance to proteins, cells, bacteria, and other micro/macroorganisms, 5,33-36 it remains a great challenge to quantify in real-time the changes in the dynamic and interactive behavior of the polymer brush, interfacial water, and protein conformation/ orientation at the polymer/water/protein interface. Computer simulations can provide further insights into the structural, dynamical, and interaction properties at polymer-water and polymer-protein interfaces with an atomic resolution that is difficult to achieve experimentally. While there are some computational studies of zwitterionic polymer systems with the main focus on the surface hydration and protein interaction of zwitterionic monomers37,38 and zwitterionic-terminated selfassembled monolayers,4 the antifouling mechanism of zwitterionic monomer-grafted membranes, 39,40 and the antifouling and mechanical properties of zwitterionic hydrogels⁴¹ using molecular dynamics (MD) simulations, very few studies have been conducted to simulate the protein adsorption/desorption on zwitterionic brushes in the presence of explicit water. Early molecular simulations of zwitterionic materials mainly focused on the interfacial water behaviors on PC-terminated selfassembled monolayers (PC-SAMs), in comparison with EG-, OH-, and CH₃-terminated SAMs. 42-44 It was found that hydrophilic or zwitterionic-terminated SAMs including EG-, OH-, and PC-SAMs induced a stronger interaction with interfacial water molecules than hydrophobic CH₃-SAMs, ^{25,43,45-47} indicating that surface hydration is considered as a crucial factor for antifouling performance because the strong hydration layer near the surface prevents the adhesion of foreign substances. Later, with a significant increase in computer power, MD simulations allowed researchers to model and simulate more complex and larger polymer-grafted surfaces in the absence and presence of foulants. Cheung et al.48 applied MD simulations to examine the effect of the grafting density on the conformation and hydration properties of a series of zwitterionic "peptoid" brushes. They found that the chain flexibility and water density around peptoid brush chains were promoted by charged monomers/residues at "low" and "intermediate" grafting densities, but were suppressed at high grafting densities due to free volume effects. Liu et al.39 modelled a zwitterionic DMAPS-grafted PVDF membrane (e.g. PVDF-g-DMAPS membrane) and used this zwitterionic-coating membrane to study the fouling process of sodium alginate in water molecules and CaCl2 ions. The hydrophilic property and electrostatic repulsion of the PVDF-g-DMAPS membrane are the two dominant but competing factors to control the antifouling capability at different zwitterionic DMAPS grafting ratios. Xiang et al. 49 computationally studied the surface hydration and antifouling behavior of poly(sulfobetaine)-grafted (pSB)

brushes using steered MD simulations. They observed graftingdensity-dependent antifouling behavior, i.e., the surface resistance to a protein is attributed to the surface hydration layer on highly grafted pSB brushes, but steric repulsion as induced by protein compression on intermediate- and low-grafted pSB brushes.

While the above-mentioned simulations and experiments have examined the structural dependence of the grafting density on the surface hydration and polymer dynamics and their correlation with the antifouling performance, they all did not address the packing structure of zwitterionic polymer brushes. Since most polymer brushes are prepared via twostep surface-initiated atom transfer radical polymerization (SI-ATRP) by first coating an initiator-SAM on a gold substrate, followed by ATRP to gradually grow polymer chains to form polymer brushes with well-controlled thickness and roughness, thus the packing structure of these polymer brushes is solely determined by the packing structure of the underlying initiator-SAM on the gold substrate, in which polymer chains have been often assumed to adopt the conventional $\sqrt{3} \times \sqrt{3R30^{\circ}}$ lattice structure with a chain-chain separation distance of 4.95 Å via typical sulfur-gold (S-Au) bonds. Such a conventional $\sqrt{3}$ × $\sqrt{3R30^{\circ}}$ lattice structure can well describe the packing structure of polymer brushes with small terminal or pendant groups (e.g., -CH₃, -EG, -OH, and COOH). However, it still remains unknown whether this small lattice structure can be also applied to other polymer brushes with much larger pendant groups. Our previous work has found that even for rigid and short SAMs, PC-SAMs prefer to adopt a larger $\sqrt{7} \times \sqrt{7R19^{\circ}}$ lattice structure, instead of the $\sqrt{3} \times \sqrt{3R30^{\circ}}$ lattice structure, due to the larger size and stronger polarity of zwitterionic PC groups.44

Currently, there is little information on the packing structure of zwitterionic polymer brushes, which prevents better understanding of the structure dependent relationship between surface hydration and protein resistance on the molecular scale. To bridge this gap, herein we performed different molecular dynamics simulations to computationally study the packing structure, surface hydration, and surface resistance to a protein of three zwitterionic polymer brushes of poly(carboxybetaine methacrylate) (pCBMA), poly(sulfobetaine methacrylate) (pSBMA), and poly((2-(methacryloyloxy)ethyl)phosporylcoline) (pMPC) brushes, as well as a hydrophilic poly(ethylene glycol) (PEG) brush for comparison. Firstly, we studied and determined the optimal lattice structures of the four polymer brushes on a Au substrate in their lowest energy states from a large energy landscape using molecular mechanics (MM) simulations. Different from the PEG brush, the three zwitterionic polymer brushes are more likely to undergo large conformational changes and involve more complex inter- and intra-interactions (e.g. charge-charge, charge-dipole, and dipole-dipole interactions) due to their long side chains and the larger zwitterionic groups, both of which would require larger lattice structures to accommodate the packing structure and interactions between polymer chains. Then, upon obtaining the optimal lattice structures, the surface hydration and surface resistance to a protein of the four polymer brushes were

examined and compared using both conventional molecular dynamics (MD) and steered MD (SMD) simulations. Collective MD data from RDFs, coordination numbers, self-diffusion, and mean residence times of interfacial water molecules revealed that the pCBMA, pSBMA, and pMPC brushes had stronger and more stable interactions with interfacial water molecules than the PEG brush. SMD further demonstrated the existence of repulsive forces derived from the three zwitterionic brushes to resist protein adsorption. Among the four polymer brushes, the strength of surface hydration and protein resistance decreased in the order of pCBMA > pMPC > pSBMA > PEG. Our simulation work for the first time determined the optimal packing structure of zwitterionic brushes and provided a more accurate description of the packing structure dependent relationship between the surface hydration and antifouling property of zwitterionic polymer brushes at the atomic level, which helps to design more effective antifouling materials and coating surfaces.

2. Materials and methods

2.1. Force field parameters

We developed the CHARMM-format force field parameters of the CBMA and SBMA monomers using the ParaChem tool (https://cgenff.paramchem.org/)⁵⁰ and obtained the force field parameters of the MPC and EG monomers from both the CHARMM36 lipid parameters⁵¹ and CHARMM35 ether parameters,⁵² respectively. The molecular structures of the CBMA, SBMA, and MPC monomers are shown in Fig. 1 and their force field parameters in the CHARMM format are provided in Table S1 (ESI†). Lysozyme (LYZ, PDB ID: 7LYZ)⁵³ was selected as a model protein to study the four different brushes due to extensive studies on its adsorption behavior on different surfaces. The CHARMM27 parameter set with CMAP correction⁵⁴ was used to model lysozyme, water (TIP3P model), and counter ions.

2.2. Model construction of polymer brushes

To study the surface hydration of different polymer brushes, we constructed polymer brush models in the presence of the explicit TIP3P water model, including three zwitterionic polymer brush models (pCBMA, pSBMA, and pMPC) and a PEG model.

Fig. 1 Molecular structures of (a) carboxybetaine methacrylate (CBMA), (b) sulfobetaine methacrylate (SBMA), and (c) (2-(methacryloyloxy)ethyl)-phosporylcoline (MPC).

Table 1 Geometric parameters of the 29 unit cells for a single brush chain

Lattice name	a (Å)	b (Å)	γ (°)	Area (Ų)	Lattice name	a (Å)	b (Å)	γ (°)	Area (Ų)
3	4.995	4.995	60	21.6	9b	8.652	7.630	79.1	64.8
4a	5.768	4.995	90	28.8	10a	9.990	10.398	43.9	72.0
4b	5.768	5.768	60	28.8	10b	10.398	7.630	65.2	72.0
5	7.630	4.995	70.9	36.0	10c	7.630	9.990	70.9	72.0
6a	8.652	4.995	90	43.2	10d	14.420	4.995	90	72.0
6b	9.990	4.995	60	43.2	10e	14.420	5.768	60	72.0
6c	8.652	5.768	60	43.2	10f	15.260	4.995	70.9	72.0
6d	5.768	7.630	79.1	43.2	11a	12.570	7.630	55.8	79.3
7	7.630	7.630	60	50.4	11b	7.630	10.398	90	79.3
8a	11.536	4.995	90	57.6	12a	11.360	8.652	61.6	86.4
8b	11.536	5.768	60	57.6	12b	8.652	10.398	73.9	86.4
8c	10.398	5.768	73.9	57.6	12c	14.980	7.630	48.2	86.4
8d	9.990	7.630	49.1	57.6	12d	11.360	7.630	85.6	86.4
8e	9.990	5.768	90	57.6	12e	8.652	9.990	90	86.4
9a	8.652	8.652	60	64.8					

For any given polymer brush model, a single chain was firstly constructed by connecting 5 repeated carboxybetaine methacrylate (CBMA), sulfobetaine methacrylate (SBMA), (2-(methacryloyloxy)ethyl)phosporylcoline (MPC), or ethylene glycol (EG) monomers to an initiator on Au and then energy minimized in a vacuum. Then, we applied molecular mechanics (MM) simulations to determine the optimal packing structure of the different brushes. The optimal packing structure of these brushes primarily depends on the packing density and the orientation of brush chains. For any given minimized single chain of a zwitterionic polymer or PEG brush, we created a 6 × 6 array of brush chains to model the packing structure of the various polymer brushes by using 29 unit cells as a basic building block to describe their different packing densities and by rotating the polymer chains from 0 to 360° in 30° steps to describe different chain orientations. Table 1 summarizes the 29 unit cells and the corresponding geometric parameters $(a, b, \gamma, and the unit area)$, where a and b are the two vector lengths of the different lattice structures and γ is the angle between a and b. The optimal packing structures of the four polymer brushes were determined in the lowest-energy state by comparing all possible packing structures from a combination of 29 unit cells and 12 chain rotations. Based on the optimal packing structure obtained above, we further created much larger-size polymer brushes using a 15 \times 9 array for the zwitterionic polymer brushes (135 zwitterionic polymer brush chains) and a 15 \times 15 array for PEG (225 PEG chains) in the presence of explicit TIP3P water molecules to study their surface hydration properties.

2.3. Model construction of polymer brushes in the presence of a protein

Based on the optimal packing structures of the four polymer brushes, we will further examine the surface resistance ability to a protein of the four polymer brushes by constructing four polymer–protein models of the polymer brushes with lysozyme (pCBMA-LYZ, pSBMA-LYZ, pMPC-LYZ, and PEG-LYZ) in the presence of explicit TIP3P water molecules and counter ions of NaCl. The calculated ionic strength was 1.85, 1.54, and 1.54 mol L⁻¹ for the pCBMA, pSBMA, and pMPC systems,

respectively, which appears to be much higher than the ionic strength of 0.295 mol L⁻¹ in PBS solution. First, Monte Carlo (MC) simulations were performed to determine the optimal orientations of lysozyme on the different zwitterionic and PEG brushes. All polymer brushes were firstly energy minimized in the implicit solvent model while fixing the sulfur atoms of the initiators by using the conjugate gradient method for 1000 steps. Then, lysozyme was placed at various separation distances of 3 to 10 Å above the minimized brushes with a random, initial orientation. During the MC simulations, at a given separation distance between lysozyme and the polymer brushes, lysozyme was allowed to rotate freely around its center of mass for 5000 steps to find its optimal orientation on the different polymer brushes, where the brush surfaces were constrained in the x-y plane. The optimal orientation of lysozyme on the distinct polymer brushes was determined as the lowest interaction energy state between the brush and lysozyme. Upon determining the optimal orientation of lysozyme on each polymer brush, these lysozyme-brush configurations will be used as a starting pose to further study the adsorption process of lysozyme on different brushes using molecular dynamics (MD) simulations and the surface resistance ability (i.e. repulsive force) of different brushes to lysozyme using steered molecular dynamics (SMD) simulations. The details of the MD and SMD simulations of lysozyme on polymer brushes are described below.

From a modeling viewpoint, our and other brush models were constructed with perfect flatness to eliminate any surface roughness effect on the surface hydration and protein resistance. The average brush heights for the three zwitterionic brushes were well retained at a constant value, with almost undetectable fluctuation (data not shown). Without surface roughness, molecular simulations can truly reflect the intrinsic antifouling property of the polymer brush itself. From an experimental viewpoint, surface roughness is always a factor to influence surface hydration and protein interactions. We and other researchers have reported that either a flat surface or nanopatterned surfaces have much better antifouling performance than randomized surface roughness. 55-59

2.4. MD simulation details

Prior to equilibrium and production MD simulations, multiple energy minimizations were performed to remove bad contacts and relax the systems for each polymer brush model with or without lysozyme: (i) conjugate gradient minimization was performed by constraining the brush chains and lysozyme to relax the water molecules for 5000 steps; (ii) an additional 5000step minimization was carried out to relax all atoms with fixing only sulfur atoms; (iii) a short 0.5 ns MD simulation with a time step of 1 fs was conducted to relax the water molecules and ions with the atoms of the brush chains and lysozyme being fixed; and (iv) another 0.5 ns MD simulation was performed with fixing sulfur atoms at a time step of 1 fs.

For conventional MD simulations, they were performed using the all-atom NAMD 2.12 package⁵⁴ with the CHARMM force field under the NVT (constant number of atoms, constant volume, and constant temperature) ensemble and 3D periodic boundary conditions. The temperature was maintained at 298 K using the Langevin thermostat method with a damping coefficient of 1 ps⁻¹. All covalent bonds including hydrogen bonds were constrained by the RATTLE method, so that the velocity Verlet method was performed to integrate Newton's equations of motion with a larger timestep of 2 fs. For the SMD simulations, lysozyme was firstly placed above the brushes with a separation distance of 14 Å. Then, a harmonic force with a force constant of 15 kcal (mol A²)⁻¹ was applied to the center of mass of lysozyme by pulling lysozyme towards the brushes at a constant velocity of 0.05 m s⁻¹ using the NAMD 2.12 package.⁵⁴ During this pulling process, the total force acting on lysozyme was recorded in real-time. For both the MD and SMD simulations, long-range electrostatic potentials were calculated by the Particle Mesh Ewald (PME) method with a grid space of 0.5 Å, while shortrange van der Waals (vdW) potentials were estimated by a switching function with a twin-range cutoff at 12 Å and 14 Å. All MD trajectories were saved every 2 ps for further analysis.

3. Result and discussion

Optimal packing structures of the zwitterionic polymer and PEG brushes

The packing structure of a polymer brush is generally described by the packing density and chain orientation, both of which are critical for the physicochemical properties of the polymer brush.60 Briefly, regarding the packing density, we first used a total of twenty-nine unit cells with different sizes and shapes to separately construct twenty-nine 6×6 assays (containing 36) polymer chains) to model the different packing densities of the four polymer brushes. Fig. 2 shows the twenty-nine unit cells and Table 1 summarizes their geometric parameters $(a, b, and \gamma)$. Each unit cell is denoted by a number and a letter, where the number represents the number of Au atoms (solid cycles) in the unit cell and the letter is used to distinguish different unit cells under the same number of Au atoms. Then, to consider the chain orientation effect for any given packing density of the polymer brush, we further rotated 36 polymer chains from 0° to 360° in 30° steps to describe different chain orientations. Thus, for a given polymer brush, a total of 348 packing structures were constructed and their packing energies were calculated and compared using MM.

Fig. 3 shows the packing energies of the three zwitterionic polymer (pCBMA, pSBMA, and pMPC) and one PEG brushes as a function of the unit cells with the already determined optimal chain orientations from MM simulations. As shown in Fig. 3, for all brush systems, there existed an optimal unit cell to better accommodate the brush chains driven by the most energetically favorable chain-chain interactions. Generally, the polymer brushes packed with too small unit cells (e.g. 3, 4a, 4b, and 5) led to unfavorable packing interactions due to the steric overpacking effect between large pendant groups, while the brushes with too large unit cells (e.g. 11a, 11b, 12a, 12b, 12c, 12d, and 12e) also lost some van der Waals (vdW) interactions due to the large

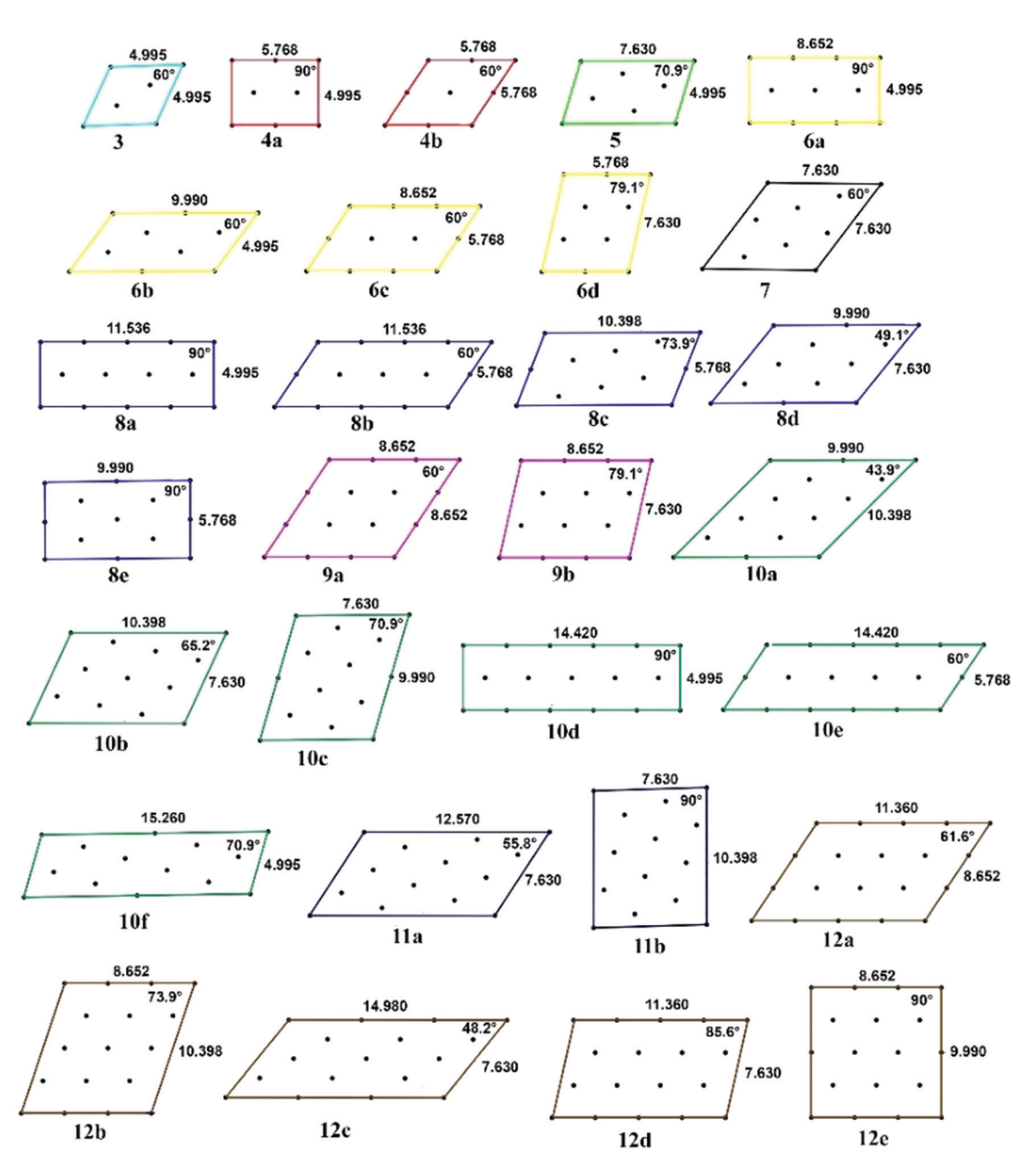


Fig. 2 Schematic of the twenty-nine unit cells used to accommodate a single chain and to present the packing density of the polymer brushes. All of the unit cells are defined by their lattice structural parameters (a, b, γ) and unit area as shown in this figure and listed in Table 1. Each unit cell is denoted by an integer and a letter, where an integer represents the number of Au atoms (solid circles) per unit cell and a letter represents each distinct unit cell containing the same number of Au atoms.

separation distance between polymer chains. On the other hand, the three zwitterionic polymer brushes (pCBMA, pSBMA, and pMPC) adopted distinct packing structures, showing a structure-dependent behavior. pCBMA containing two ethylene groups between zwitterionic groups reached the lowest packing energy for the unit cell of 10b with an optimal chain orientation of 330°, while pSBMA and pMPC with three ethylene groups between zwitterionic groups preferred to adopt the larger unit cells of 12c and 12a with optimal chain orientations of 30° and 60°, respectively. Completely different from the three zwitterionic brushes, the PEG brush with small ethylene glycol groups

demonstrated an energetical preference to adopt a typical $\sqrt{3} \times \sqrt{3}R30^{\circ}$ configuration with a chain orientation of 30° , consistent with several previous studies. As a result, the packing density was 72.0 Å² per pCBMA chain, 86.4 Å² per pSBMA chain, and 86.4 Å² per pMPC chain, all of which are 3–4 times larger than the packing density of PEG brushes (*i.e.*, 21.6 Å² per PEG chain).

3.2. Interfacial water structures and dynamics on polymer brushes

On the basis of the "water barrier" hypothesis, it is generally accepted that the tightly bonded water layer near polymer

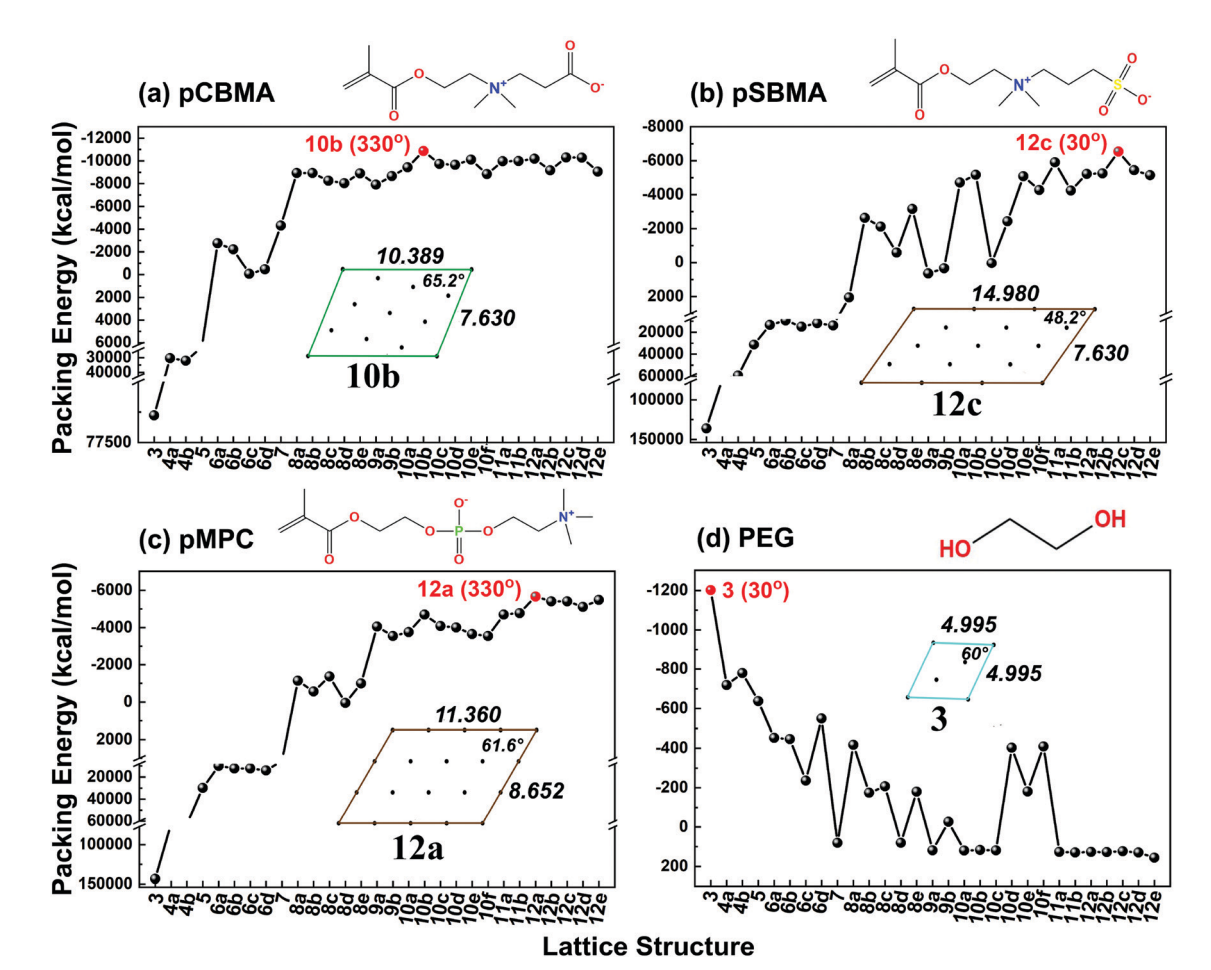


Fig. 3 Searching for the optimal packing structures (red circles) of the three zwitterionic and one PEG brushes. Packing energies of the (a) pCBMA, (b) pSBMA, (c) pMPC, and (d) PEG brushes as a function of the unit cells with already determined optimal chain orientation of polymer chains. For each unit cell, the brush chain orientation is considered by varying from 0° to 360° with an increase of 30°

brushes is critical for the antifouling performance, because structured and dynamic water at interfaces can greatly mediate protein adsorption.⁶² Since it is not possible to use single or simple parameters derived from water behavior to correlate well the strength of bound water molecules to polymer chains with protein adsorption, the binding behavior of interfacial water molecules to polymer chains is characterized and measured using the radial distribution function (RDF),

coordination number, orientation distribution, residence time, and self-diffusion coefficients of water molecules on polymer brushes.

Fig. 4a shows the radial distribution functions (RDFs) of interfacial water molecules on the pCBMA, pSBMA, pMPC, and PEG brushes, where the RDF presents the ratio of the local water density to the bulk water density as a function of the distance from the reference groups of the polymer brushes.

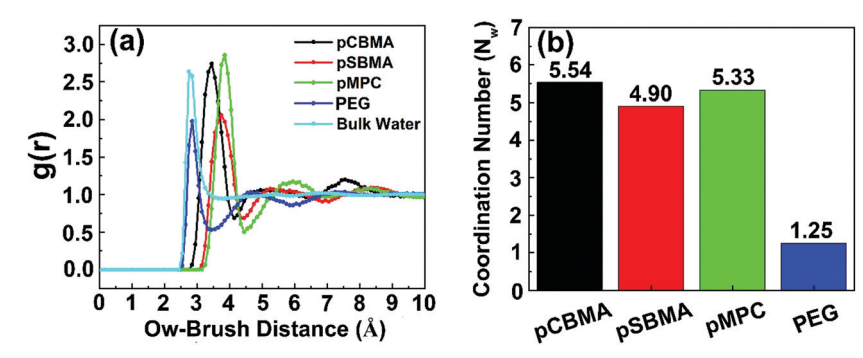


Fig. 4 Interfacial water structures on the four polymer brushes. (a) RDFs and (b) coordination number (N_w) of interfacial water molecules on the pCBMA, pSBMA, pMPC, and PEG brushes.

Oxygen atoms from the PEG brush and zwitterionic groups (CO₂⁻, SO₃⁻, or PO₄⁻) from the corresponding pCBMA, pSBMA, pMPC brushes were selected as the reference points for the RDFs. At first glance, all pCBMA, pSBMA, pMPC, and PEG brushes exhibited two major peaks (i.e. first/second peaks) at locations of 3.40/4.85 Å, 3.55/5.32 Å, 3.85/5.95 Å, and 2.85/ 4.75 Å, respectively, where the first hydration peak was much more pronounced than the second one, indicating more water molecules in the first hydration layer than the second hydration layer. While the pCBMA, pSBMA, and pMPC brushes had similar reference points of CO₂⁻, SO₃⁻, and PO₄⁻, the two peak locations showed an increasing order of pCBMA > pSBMA > pMPC. The packing density can also influence the distribution of water molecules at the surface. Along with the fact that the pCBMA brush has a higher packing density than the pSBMA and pMPC brushes, the shift of the hydration peaks indicates that as compared to the relatively loosely packed pSBMA and pMPC brushes, water molecules are still inclined to penetrate into the tightly packed pCBMA brush to form a more enriched hydration layer at the pCBMA surface. Next, in Fig. 4b, we quantified the coordination number (N_w) of interfacial water molecules of pCBMA, pSBMA, pMPC, and PEG by integrating the first hydration shell of the RDFs from Fig. 4a. It can be seen in Fig. 4b that $N_{\rm w}$ around the pCBMA, pSBMA, and pMPC brushes was 5.54, 4.90, and 5.33, respectively, which were much higher than $N_{\rm w}$ = 1.25 for PEG, confirming that zwitterionic moieties (e.g. -CB, -SB, and -PC) can induce much stronger surface hydration than the EG group. We attribute the structural differences in the RDF shift and $N_{\rm w}$ between the zwitterionic brushes and hydrophilic brushes to the different solvation mode, i.e., ionic solvation of zwitterionic polymer brushes induces a stronger hydration strength than hydrogen bonding solvation of hydrophilic polymer brushes.

To characterize the orientation distribution of water molecules on the four different polymer brushes, we defined an angle θ between the dipole moment of water molecules and the brush normal, as illustrated in Fig. 5a, where 0° (H-down) or 180° (H-up) indicates that a water molecule orients vertically relative to the surface with two hydrogens pointing towards or

away from the surface, while 90° indicates that a water molecule lies parallel to the surface. Fig. 5b shows the orientation distribution of water molecules (θ) in the first hydration layer around the four different polymer brushes. As a control, θ obtained from bulk water had a broad and almost flat distribution, indicating a random orientation distribution of water molecules in the bulk. The four θ profiles on the polymer brushes displayed a single dominant peak, but with different maximal θ values, *i.e.*, $\theta_{\text{max}} = 100^{\circ}$, 100° , 130° , and 110° for the pCBMA, pSBMA, pMPC, and PEG brushes, respectively. Since the PEG brush tends to interact with water molecules via hydrogen bonds between oxygen atoms in EG groups and hydrogen atoms in water, interfacial water molecules had both H-up and H-down orientations on the surface. Differently, H-down oriented water molecules were preferentially located on the pCMBA and pSBMA brushes, while H-up oriented water molecules tended to sit on the phosphate groups of the pMPC brush (Fig. 5b). Either case demonstrates a highly ordered behavior of water molecules occurring at the interface. Such a difference in the θ profiles is another indicator that interfacial water molecules adopt certain highly populated orientations to interact with polymer brushes relative to disordered bulk water.

Since the preferential water orientation is strongly dependent on the surface chemistry and structure of the polymer brushes, we further quantified the structural orientation of the terminal zwitterionic groups of the pCBMA ($\mathrm{CO_2}^-$ and $\mathrm{NC_4}^+$), pSBMA ($\mathrm{SO_3}^-$ and $\mathrm{NC_4}^+$), and pMPC ($\mathrm{PO_4}^-$ and $\mathrm{NC_4}^+$) brushes. We defined an angle φ between the dipole moment of the terminal zwitterionic moieties and the brush normal to quantify the average orientation of all zwitterionic moieties in the brushes (Fig. 6a). The dipole moment of the terminal zwitterionic moieties was defined as the positive groups ($\mathrm{NC_4}^+$) orientating towards the negative groups ($\mathrm{CO_2}^-$, $\mathrm{SO_3}^-$, and $\mathrm{PO_4}^-$) of pCBMA, pSBMA, and pMPC.

The distribution probability profiles of φ in Fig. 6b showed that the highly populated φ for pCBMA, pSBMA, and pMPC peaked at 60°–90°, 90°, and 130°, respectively. Despite the difference in φ , further visual inspection of the MD trajectories showed that all zwitterionic brushes formed a well-defined

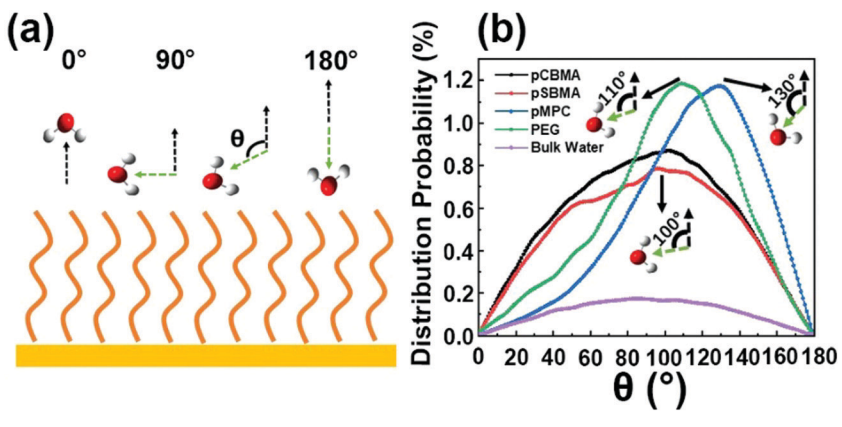


Fig. 5 Water orientation distribution (θ) on the pCBMA, pSBMA, pMPC, and PEG brushes. (a) Definition and (b) distribution probability of θ in the first hydration layer of the four polymer brushes.

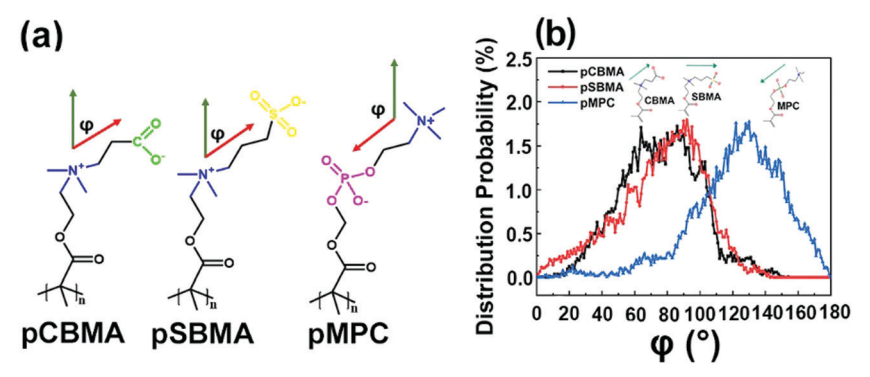


Fig. 6 Dipole orientations of zwitterionic groups in the pCBMA, pSBMA, and pMPC brushes. (a) Definition and (b) dipole distribution probability (%) of φ for the pCBMA, pSMBA, and pMPC brushes. φ is the angle between the dipole of the zwitterionic groups of pCBMA (60°-90°), pSBMA (90°), and pMPC (130°) and the brush normal

layer with a relatively uniform thickness and top surface. It appeared that the zwitterionic groups dominated the chain orientation to retain the extended brush conformations. Meanwhile, to minimize the zwitterionic group-induced dipole on the brush surfaces, the zwitterionic groups tended to adjust their orientations to have specific interactions with water molecules. The pCBMA brush had an up-tilted orientation of 60°-90° to facilitate negatively charged CO₂ groups to interact with positively charged hydrogen atoms of water molecules. The pSBMA brush adopted an almost parallel orientation to the surface, which exposed more negatively charged sulfonate groups and hydrophobic CH2 groups at the water-zwitterion interface while allowing the positively charged quaternary ammonium groups to stay largely in the inner region of the brush. Differently, pMPC (130°) had a completely opposite dipole to pCBMA (60°-90°) and pSBMA (90°) and thus pMPC adopted a down-tilted orientation of 130° to better accommodate water molecules to form a dense dipole network between the positively charged NC₄⁺ group of pMPC and negatively charged oxygen atoms of interfacial water molecules. Overall, comparison of the distribution probability of the water orientation (θ) in Fig. 5b with the dipole distribution of zwitterionic groups (φ) in Fig. 6b confirms the formation of an interfacial dipole network between zwitterionic groups and water molecules in the first hydration shell, which acts to minimize the surface dipoles and charges to enhance the surface hydration and possibly suppress electrostatic/dipole-induced protein adsorption. A number of studies have shown that water molecules adopted both H-down and H-up orientations at the zwitterionic POPC/water interface. 63,64 Water strongly associated with the negatively charged PO₄⁻ with H-up orientation exhibited relatively stronger H-bond interactions with the zwitterionic surface than that associated with positively charged NC₄⁺ with H-down orientation, presumably due to the higher charge density of the PO₄⁻ group (-1.2e) than the NC₄⁺ group (+0.78e). It was also reported that positively charged surfaces are more favorable to interact with oxygen atoms of water molecules, while negatively charged surfaces tend to interact with hydrogen atoms of water molecules, 65,66 highlighting the importance of the surface chemistry of the brushes in the water orientation.

From a dynamic viewpoint of the water hydration shell around the different zwitterionic polymer brushes, we applied the mean residence time (MRT, Fig. 7a) and self-diffusion coefficient (SDC, Fig. 7b) to characterize the dynamics of interfacial water molecules in the first hydration layer of the four brushes. MRT (τ_s) is obtained by fitting an autocorrelation func-

tion of
$$C_R(t) = \frac{1}{N_{\rm w}} \sum_{j=1}^{N_{\rm w}} \frac{\left\langle P_{Rj}(0) P_{Rj}(t) \right\rangle}{\left\langle P_{Rj}(0)^2 \right\rangle}$$
 with $C_R(t) = A \exp\left(-\frac{t}{\tau_{\rm s}}\right)$,

where P_{Rj} is a binary function and the value of 0 (1) means that the jth water molecules stays in (leaves) a layer with a thickness of R at a time of t. A longer residence time (τ_s) indicates more stable water-polymer interactions, and vice versa. As shown in Fig. 7a, the residence times of interfacial water molecules in the first hydration layer of pCBMA, pSBMA, pMPC, and PEG, as derived from the decay in the lifetime autocorrelation function, were 480 ps, 132 ps, 306 ps, and 63 ps, respectively, all of which were much longer than the residence time of water molecules in the bulk (40 ps), indicating more stable association between the polymers and water than water-water interactions. Water molecules bound to the three zwitterionic brushes also exhibited 2–8 times longer τ_s than those bound to the PEG brush, indicating that ionic solvation as induced by zwitterionic groups imposes stronger interactions with water molecules than hydrogen bonds as induced by hydrophilic groups. The residence time is also strongly dependent on the electrostatic interactions between water molecules and the anionic groups, which rely on the charge densities of the anionic groups. Thus, we observed that τ_s for the three zwitterionic brushes exhibited a decreasing order of pCBMA > pMPC > pSBMA, consistent with the coordination numbers of water molecules around the zwitterionic brushes. In addition, the carbon space length (CSL) may also affect the hydration structure and dynamic properties of these three zwitterionic groups. pCBMA and pMPC with CSL = 2 between zwitterionic groups had a longer τ_s of interfacial water molecules than pSBMA with CSL = 3, probably because the smaller CSL = 2 allows water molecules to form a bridge hydration layer between zwitterionic

In parallel to τ_s , dynamic, surface-bound water molecules will be slowed by nearly any surface and the degree of slowing can be measured by the water self-diffusion coefficient (SDC).

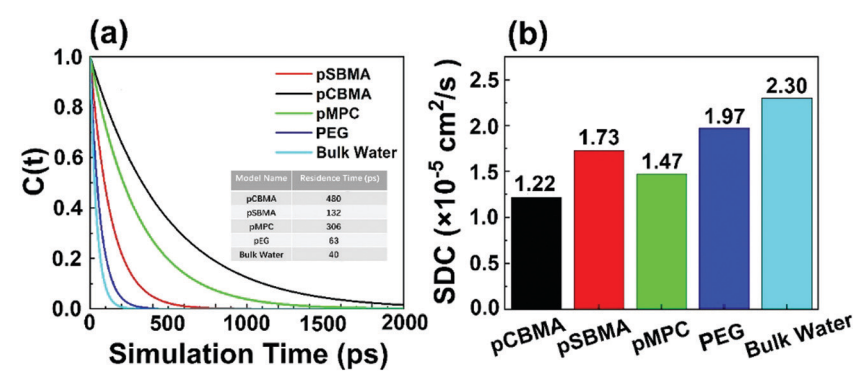


Fig. 7 Interfacial water dynamics on polymer brushes. (a) Mean residence time (τ_s) and (b) self-diffusion coefficients (SDC) of interfacial water molecules in the first hydration shell of the pCBMA, pSMBA, pMPC, and PEG brushes.

Herein, we also examined the self-diffusion coefficient (SDC) of interfacial water molecules in the first hydration layer of the pCBMA, pSBMA, pMPC, and PEG brushes by fitting a function of SDC = $\lim_{t\to\infty}\frac{1}{6t}\langle [r_j(t)-r_j(0)]^2\rangle$, where $r_i(t)$ and $r_i(0)$ are the coordinates of the jth atom at a time of t and 0, respectively, and $\langle\cdots\rangle$ indicates the ensemble average. As shown in Fig. 7b, pCBMA, pSBMA, pMPC, and PEG exhibited a smaller SDC of 1.22×10^{-5} cm² s⁻¹, 1.73×10^{-5} cm² s⁻¹, 1.47×10^{-5} cm² s⁻¹, and 1.97×10^{-5} cm² s⁻¹ than bulk water (2.30×10^{-5} cm² s⁻¹), suggesting that all polymer brushes slow down water diffusion considerably as compared to the diffusion of bulk water. Among the four brushes, PEG-bound water molecules are more dynamic than zwitterionic-brush bound water molecules, as evidenced by the shorter τ_s and the larger SDC.

Obviously, the packing structure and surface chemistry of the zwitterionic brushes (e.g. hydrophobicity/hydrophilicity ratio, charge distributions of cationic and anionic groups, and intra- or inter-chain interactions between zwitterionic groups) greatly contribute to the structure and dynamics of water molecules, which are essential for understanding surface hydration and the underlying polymer-water interactions. Collective simulation data from the RDFs, coordination number, residence time, and self-diffusive coefficient showed consistent results on the structure and dynamics of interfacial water molecules. The zwitterionic brushes, particularly pCBMA, not only bind more water molecules but also bind them stronger and longer than the PEG brush, confirming that zwitterionic groups induce stronger surface hydration than hydrophilic groups. Among the three zwitterionic brushes, the different hydration properties are attributed to both zwitterionic groups and CSLs in zwitterionic polymer chains. Previous studies have shown that the hydration free energy and charge density of NC₄-CO₂ $(-261 \pm 12 \text{ kJ mol}^{-1} \text{ and } -5.3e \text{ nm}^{-3})$ were smaller than NC₄-SO₃ ($-251 \pm 17 \text{ kJ mol}^{-1}$ and $-4.5e \text{ nm}^{-3}$), indicating stronger surface free energy of -CB moieties than -SB moieties.^{37,67} In addition, the simulation results also showed the impact of CSL-induced surface hydration. pCBMA has a CSL of 2 between CO_2^- and NC_4^+ groups, while pSBMA and pMPC have a CSL of 3 between SO₃⁻ and NC₄⁺ and between PO₄⁻ and NC₄⁺. The increase of the CSL will increase the hydrophobicity/hydrophilicity ratio of zwitterionic chains and alter the chain flexibility, both of which would lead to different water–polymer interactions, inducing different surface hydration and antifouling behaviors for different polymer brushes. Also, CSL = 2 in pCBMA has a separation distance of 3.8 Å, which allows water molecules to form bridging bonds between the two adjacent $\mathrm{CO_2}^-$ and $\mathrm{NC_4}^+$ groups.

3.3. Protein adsorption/desorption on polymer brushes

Lysozyme is selected as a model foulant protein to quantify the degree of surface resistance of the zwitterionic and PEG brushes. The protein adsorption process demands a long timescale of seconds to hours in experiments, which is far beyond the timescale of 100 ns-us of conventional molecular dynamics.68 To overcome this timescale issue, we proposed two different computational strategies to study the lysozyme adsorption process on the polymer brushes. The first strategy is to use a combination of Monte Carlo (MC) and MD simulations to study the lysozyme adsorption/desorption process on the different polymer brushes, in which MC simulations were first performed to determine the optimal orientation of lysozyme on the polymer brushes, followed by all-atom, explicit-water MD simulations to determine the surface resistance to lysozyme. Fig. 8 shows that after two million steps of MC simulations, the optimal orientations of lysozyme on the pCBMA, pSBMA, pMPC, and PEG brushes were determined in their lowest energy states.

Upon, at the lowest-energy state, lysozyme adopted a similar orientation with the V-shape region of lysozyme oriented away from the three zwitterionic polymer brushes (Fig. 8). However, we can also observe that lysozyme on PEG adopted a different orientation from the other three cases, with the V-shape region of lysozyme orientated towards the surface. Further, we characterized the residues of lysozyme orientating towards the brushes (Table 2). As shown in Table 2, some common residues of Arg₁₂₅, Gly₁₂₆, Cys₁₂₇, and Arg₁₂₈ were found to face towards the pCBMA and pSBMA brushes, which differed from the residue sequence of Thr₁₁₈-Asp₁₁₉-Gln₁₂₁-Ala₁₂₂-Trp₁₂₃-Ile₁₂₄-Arg₁₂₅ orientating towards the pMPC brush. All the above-mentioned residues were unstructured coils when facing the zwitterionic

Paper

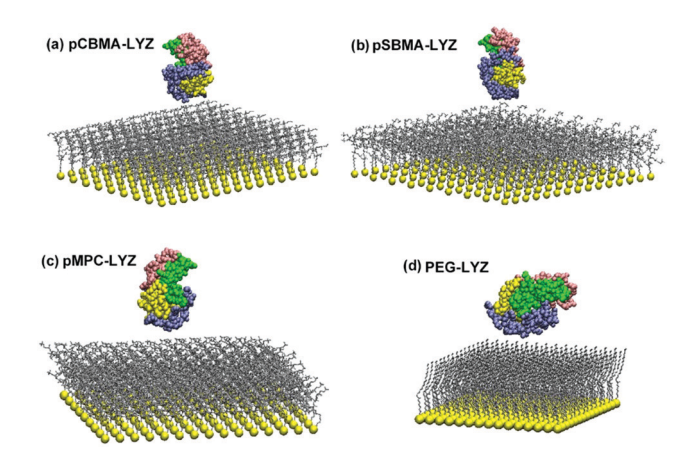


Fig. 8 Optimal orientations of lysozyme on the (a) pCBMA, (b) pSBMA, (c) pMPC, and (d) PEG brushes in the lowest energy state, as determined by MC simulations

brushes. Differently, the PEG brush induced lysozyme to orient with two regions of Thr₁₁₈-Asp₁₁₉-Gln₁₂₁-Ala₁₂₂-Trp₁₂₃-Ile₁₂₄-Arg₁₂₅ (random coils) and Arg₂₁-Gly₂₂-Tyr₂₃-Ser₂₄-Leu₂₅ (α-helical structure) towards the surface.

Upon obtaining the optimal orientations of lysozyme on each polymer brush from MC simulations, we initiated the MD simulations by placing lysozyme above the brush surface with a short separation distance of ~ 4 Å, which aims to mimic a pre-adsorption state. In this way, lysozyme is required to overcome a lower energy barrier in order to achieve its adsorption. If lysozyme is still rejected by the polymer brushes, this further confirms the strong surface resistance property of a given polymer brush. Fig. 9 shows the relative positions of lysozyme relative to the pCBMA, pSBMA, pMPC, and PEG surfaces as a function of simulation time, and final MD snapshots are also given to present the overall outcome of the adsorption process. Visual inspection of 80 ns MD trajectories showed that as the simulation began, lysozyme was quickly desorbed from the three zwitterionic brushes, as indicated by a large separation distance of 10-20 Å within 10 ns and a final separation distance of 20-70 Å at 80 ns (Fig. 9a-c), indicating the strong surface resistance of the zwitterionic brushes to lysozyme. In Fig. 9d, different from the zwitterionic brushes, lysozyme initially tended to weakly stay on the surface of the PEG brush, as evidenced by a short separation distance of 0 to 5 Å within the first 45 ns. But after 45 ns, lysozyme gradually moved away from the PEG brush. Furthermore, due to the desorption of lysozyme from the four polymer brushes, the secondary and tertiary structures of lysozyme were largely maintained.

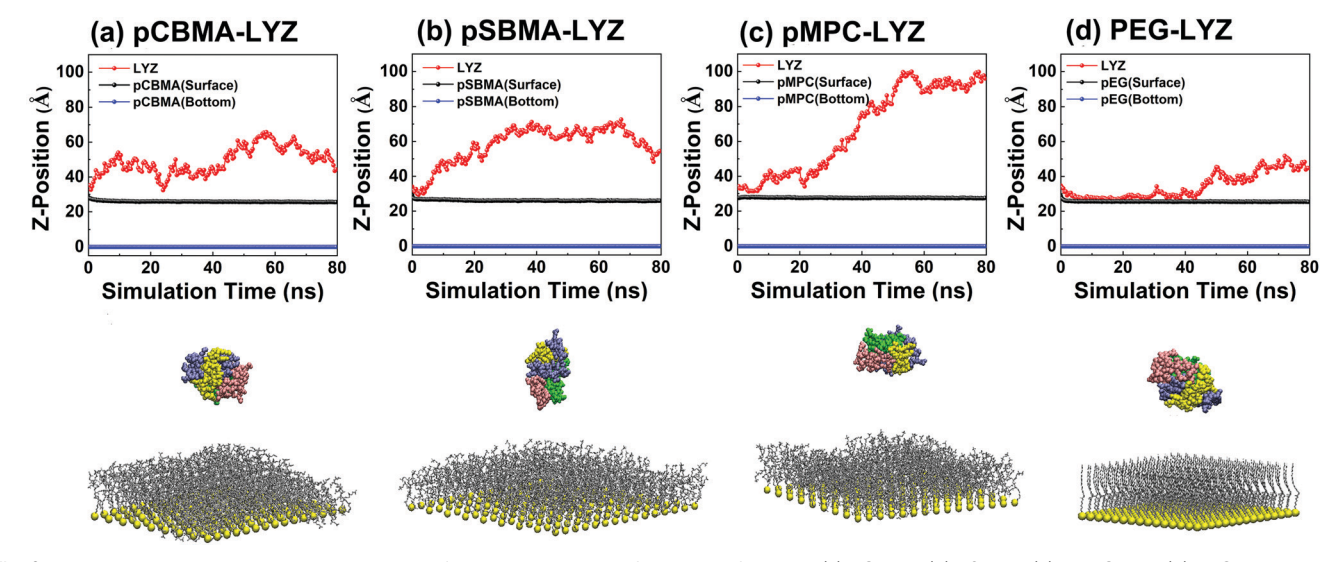
We further proposed and implemented the second computational strategy to study the surface resistance ability to

lysozyme using steered molecular dynamics (SMD) simulations. Fig. 10a illustrates the dynamical process of lysozyme approaching the polymer brushes from 14 Å to immediate contact with the pCMBA, pSBMA, pMPC, and PEG brushes at a speed of 0.05 m s⁻¹ by applying a harmonic force on the mass center of lysozyme. The driving speed of 0.05 m s⁻¹ is slow enough to ensure an approximately quasistatic approach to the surface. During this process, the potential of mean force (PMF) can be obtained (Fig. 10b) through the umbrella sampling method. As shown in Fig. 10b, for all polymer brushes, there was no repulsive force or attractive force acting on lysozyme when the separation distance between lysozyme and the surface was larger than 9 Å. The nearly zero and flat force profiles also indicate that lysozyme can readily approach any polymer brush without any anomalously high barriers. However, as lysozyme started to approach the brush surfaces from 14 Å to immediate contact with pCBMA and pMPC, the pCBMA and pMPC brushes exhibited a significant increase of repulsive forces from 0 to -7000 pN and 0 to -5500 pN, respectively, indicating the strong surface resistance of both the pCBMA and pMPC brushes to lysozyme adsorption. Differently, the repulsive forces against lysozyme adsorption from the pSBMA and PEG brushes were largely reduced to -2000 and -1000 pN, respectively, indicating that the energy barriers for protein adsorption became much less pronounced.

To better understand the origin of the repulsive forces from the polymer brushes, we further analyzed the repulsive force at two special locations of the hydration layers at which the repulsive force begins to dramatically increase. As shown in Fig. 10c, the repulsive force on lysozyme at the first/second hydration layers was -2500/-700 pN for pCBMA, -500/-200 pN for pSBMA, -2500/-500 pN for pMPC, and -200/0 pN for PEG. This indicates that (1) the force needed for lysozyme to break through the 2nd hydration layers was much smaller than that to break through the 1st hydration layers; (2) the hydration layer indeed provides a physical and energetic barrier against protein adsorption; and (3) the repulsive forces from the pCBMA and pMPC brushes were much higher than those from the pSBMA and PEG brushes at both hydration layers. Particularly, the repulsive force from the pCBMA and pMPC brushes started to increase much earlier and the increase was steeper between the two hydration layers, further highlighting the stronger association of CO₂ and PO₄ groups with water molecules than SO₃ and EG groups. A number of SPR results^{69,70} have shown that surfaces coated with pCBMA, pSBMA, and PEG brushes had protein adsorption from undiluted human blood serum/plasma of \sim 7.5/0.4 ng cm⁻², 45.1/9.1 ng cm⁻², and 87.5/>300.0 ng cm⁻², respectively, indicating that the pCBMA brush can achieve a stronger antifouling ability to reject proteins than pSBMA and

Table 2 Residues of lysozyme orientating towards the pCBMA, pSBMA, pMPC, and PEG brushes from MC simulations

	pCBMA	pSBMA	рМРС	PEG
Residues	Arg ₁₂₅ Gly ₁₂₆ Cys ₁₂₇ Arg ₁₂₈	Arg ₁₂₅ Gly ₁₂₆ Cys ₁₂₇ Arg ₁₂₈	Thr ₁₁₈ Asp ₁₁₉ Gln ₁₂₁ Ala ₁₂₂ Trp ₁₂₃ Ile ₁₂₄ Arg ₁₂₅	$\begin{array}{c} \text{Arg}_{21} \; \text{Gly}_{22} \; \text{Tyr}_{23} \; \text{Ser}_{24} \; \text{Leu}_{25} \; \text{Thr}_{118} \; \text{Asp}_{119} \\ \text{Gln}_{121} \; \text{Ala}_{122} \; \text{Trp}_{123} \; \text{Ile}_{124} \; \text{Arg}_{125} \end{array}$



Time-dependent desorption process and final MD snapshots of lysozyme from the (a) pCBMA, (b) pSBMA, (c) pMPC, and (d) PEG brushes.

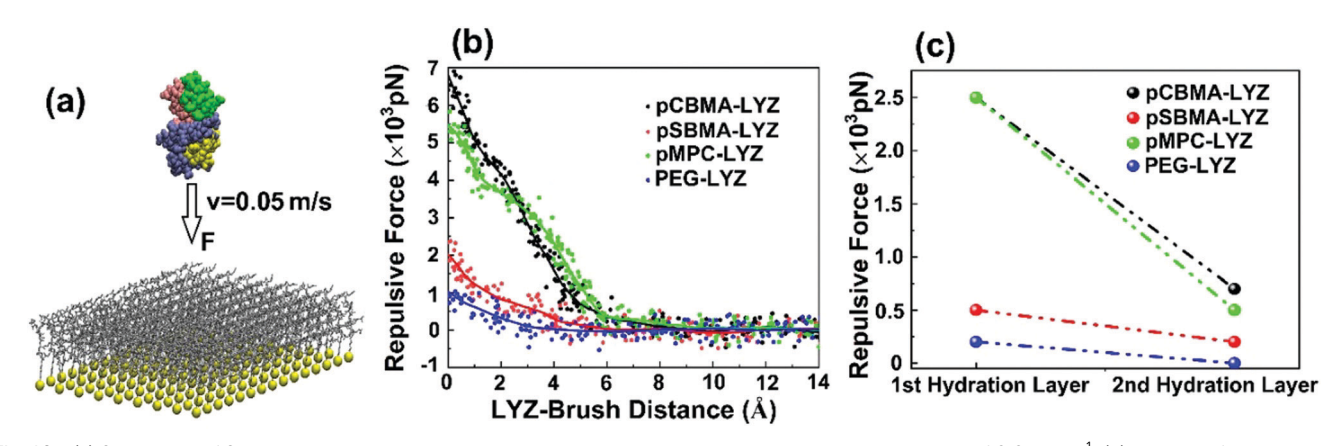


Fig. 10 (a) Schematic of SMD simulations pulling lysozyme towards polymer brushes at a constant velocity of 0.05 m s^{-1} , (b) repulsive force—distance profiles between lysozyme and the pCBMA, pSBMA, pMPC, and PEG brushes, and (c) repulsive force acting on lysozyme at the 1st and 2nd hydration layers of the pCBMA, pSBMA, pMPC, and PEG brushes.

PEG. 69-72 However, another quartz crystal microbalance (QCM) study has found that pCBMA, pSBMA, and pMPC brushes had protein adsorption of 79 ng cm⁻², 31 ng cm⁻², and 17 ng cm⁻² from undiluted fetal bovine serum, respectively, 71 suggesting that pMPC outperformed the other two zwitterionic brushes in terms of antifouling capacity. Such controversial results for the same materials but from different labs could result from different experimental conditions or measurement methods.⁷¹ Moreover, it was reported that all of the three pCBMA, pCBMA, and pMPC brushes can achieve very small water contact angles of $<20^{\circ}$, with some minor differences between them (e.g. 13-15° for pCBMA brushes, 8–10° for pMPC brushes, and 19° for pSBMA brushes).⁷¹ Considering both the simulation and experimental results together, the zwitterionic brushes exhibit stronger surface hydration and surface resistance to a protein than the PEG brush. Among the three zwitterionic brushes, the pCBMA and pMPC brushes outperform the other polymer brush to achieve the best surface

hydration and protein resistance on the basis of an optimal combination of packing structures, zwitterionic groups, and CSLs.

4. Conclusions

In this work, we computationally studied the packing structure, surface hydration, and surface resistance to a protein of three zwitterionic polymer (pCBMA, pSBMA, and pMPC) brushes, as well as a PEG brush for comparison, using MM, MC, conventional MD, and SMD simulations, where MM was used to determine the optimal packing structures of the four polymer brushes, MC to predict the optimal orientations of lysozyme on the brushes, MD to examine the surface hydration and lysozyme adoption of the brushes, and SMD to quantify the repulsive force acting on lysozyme from the brushes. Firstly, the pCBMA, pSBMA, and pMPC brushes with longer pendant sidechains energetically

preferred to adopt much larger unit cells of 10b (a = 10.395 Å, $b = 7.630 \text{ Å}, \gamma = 65.2^{\circ}, \text{ area} = 72.0 \text{ Å}^2$, 12c (a = 14.980 Å, b = 7.630 Å, b = 7.630 Å) $\gamma = 48.2^{\circ}$, area = 86.4 Å²), and 12a (a = 11.360 Å, b = 8.652 Å, $\gamma = 61.6^{\circ}$, area = 86.4 Å²), respectively, in contrast to the PEG brush with the smaller $\sqrt{3} \times \sqrt{3R30^{\circ}}$ lattice structure. Upon obtaining the optimal packing structures of the polymer brushes, collective MD simulation data from the RDFs, coordination number, dipole distribution, self-diffusion coefficient, and mean residence time of interfacial water molecules revealed the different binding strength and stability of interfacial water to different brushes, as ranked by surface hydration in terms of pCBMA > pMPC > pSBMA > PEG. Finally, a combination of MD and SMD simulation studies further confirmed that while all brushes imposed strong surface resistance to lysozyme adsorption, the repulsive force acting on lysozyme from the brushes was shown in a decreasing order of pCBMA > pMPC > pSBMA > PEG, consistent with the surface hydration order. Both orders reveal a positive relationship between surface hydration and antifouling properties of polymer brushes at the atomic level. This computational work not only shows that subtle structural changes in zwitterionic pendant groups with the same polymer backbone can greatly enhance the antifouling performance, but also provides important structure-based design principles, in which combination of zwitterionic groups with optimal CSLs could serve as a promising structural motif for the design of new effective antifouling materials beyond traditional ethylene glycol-based antifouling materials.

Conflicts of interest

There are no conflicts to declare.

Acknowledgements

This work is supported by NSF grants (DMR-1806138 and CMMI-1825122). We also thank Aristo Liu (Copley High School) for his participation in this project.

References

- 1 S. Y. Jiang and Z. Q. Cao, Ultralow-Fouling, Functionalizable, and Hydrolyzable Zwitterionic Materials and Their Derivatives for Biological Applications, Adv. Mater., 2010, 22(9), 920-932.
- 2 J. B. Schlenoff, Zwitteration: Coating Surfaces with Zwitterionic Functionality to Reduce Nonspecific Adsorption, Langmuir, 2014, 30(32), 9625-9636.
- 3 G. S. Georgiev, E. B. Kamenska, E. D. Vassileva, I. P. Kamenova, V. T. Georgieva, S. B. Iliev and I. A. Ivanov, Self-assembly, antipolyelectrolyte effect, and nonbiofouling properties of polyzwitterions, Biomacromolecules, 2006, 7(4), 1329-1334.
- 4 S. W. Xiao, B. P. Ren, L. Huang, M. X. Shen, Y. X. Zhang, M. Q. Zhong, J. T. Yang and J. Zheng, Salt-responsive zwitterionic polymer brushes with anti-polyelectrolyte property, Curr. Opin. Chem. Eng., 2018, 19, 86-93.

- 5 S. W. Xiao, Y. X. Zhang, M. X. Shen, F. Chen, P. Fan, M. Q. Zhong, B. P. Ren, J. T. Yang and J. Zheng, Structural Dependence of Salt-Responsive Polyzwitterionic Brushes with an Anti-Polyelectrolyte Effect, Langmuir, 2018, 34(1),
- 6 R. Wei, W. Y. Song, F. Yang, J. K. Zhou, M. Zhang, X. Zhang, W. F. Zhao and C. S. Zhao, Bidirectionally pH-Responsive Zwitterionic Polymer Hydrogels with Switchable Selective Adsorption Capacities for Anionic and Cationic Dyes, Ind. Eng. Chem. Res., 2018, 57(24), 8209-8219.
- 7 J. Wu, C. C. He, H. C. He, C. Q. Cheng, J. Y. Zhu, Z. C. Xiao, H. Y. Zhang, X. K. Li, J. Zheng and J. Xiao, Importance of zwitterionic incorporation into polymethacrylate-based hydrogels for simultaneously improving optical transparency, oxygen permeability, and antifouling properties, J. Mater. Chem. B, 2017, 5(24), 4595-4606.
- 8 B. Cao, Q. Tang, L. L. Li, J. Humble, H. Y. Wu, L. Y. Liu and G. Cheng, Switchable Antimicrobial and Antifouling Hydrogels with Enhanced Mechanical Properties, Adv. Healthcare Mater., 2013, 2(8), 1096-1102.
- 9 A. A. Durrani, J. A. Hayward and D. Chapman, Biomembranes as Models for Polymer Surfaces. 2. The Syntheses of Reactive Species for Covalent Coupling of Phosphorylcholine to Polymer Surfaces, Biomaterials, 1986, 7(2), 121-125.
- 10 Y. Tang, J. R. Lu, A. L. Lewis, T. A. Vick and P. W. Stratford, Swelling of zwitterionic polymer films characterized by spectroscopic ellipsometry, Macromolecules, 2001, 34(25), 8768-8776.
- 11 J. X. Liu, K. G. Yang, W. Y. Shao, S. W. Li, Q. Wu, S. Zhang, Y. Y. Qu, L. H. Zhang and Y. K. Zhang, Synthesis of Zwitterionic Polymer Particles via Combined Distillation Precipitation Polymerization and Click Chemistry for Highly Efficient Enrichment of Glycopeptide, ACS Appl. Mater. Interfaces, 2016, 8(34), 22018-22024.
- 12 C. Ventura, A. J. Guerin, O. El-Zubir, A. J. Ruiz-Sanchez, L. I. Dixon, K. J. Reynolds, M. L. Dale, J. Ferguson, A. Houlton, B. R. Horrocks, A. S. Clare and D. A. Fulton, Marine antifouling performance of polymer coatings incorporating zwitterions, Biofouling, 2017, 33(10), 892-903.
- 13 S. W. Xiao, Y. Yang, M. Q. Zhong, H. Chen, Y. X. Zhang, J. T. Yang and J. Zheneg, Salt-Responsive Bilayer Hydrogels with Pseudo-Double-Network Structure Actuated by Polyelectrolyte and Antipolyelectrolyte Effects, ACS Appl. Mater. Interfaces, 2017, 9(24), 20843-20851.
- 14 S. W. Xiao, M. Z. Zhang, X. M. He, L. Huang, Y. X. Zhang, B. P. Ren, M. Q. Zhong, Y. Chang, J. T. Yang and J. Zheng, Dual Salt- and Thermoresponsive Programmable Bilayer Hydrogel Actuators with Pseudo-Interpenetrating Double-Network Structures, ACS Appl. Mater. Interfaces, 2018, **10**(25), 21642-21653.
- 15 T. Maji, S. Banerjee, Y. Biswas and T. K. Mandal, Dual-Stimuli-Responsive L-Serine-Based Zwitterionic UCST-Type Polymer with Tunable Thermosensitivity, Macromolecules, 2015, 48(14), 4957-4966.
- 16 Y. Hisamatsu, S. Banerjee, M. B. Avinash, T. Govindaraju and C. Schmuck, A Supramolecular Gel from a Quadruple

- Zwitterion that Responds to Both Acid and Base, Angew. Chem., Int. Ed., 2013, 52(48), 12550-12554.
- 17 T. Bai, S. J. Liu, F. Sun, A. Sinclair, L. Zhang, Q. Shao and S. Y. Jiang, Zwitterionic fusion in hydrogels and spontaneous and time-independent self-healing under physiological conditions, *Biomaterials*, 2014, 35(13), 3926–3933.
- 18 M. Chen, W. H. Briscoe, S. P. Armes, H. Cohen and J. Klein, Polyzwitterionic brushes: Extreme lubrication by design, *Eur. Polym. J.*, 2011, 47(4), 511–523.
- 19 M. Kobayashi, Y. Terayama, N. Hosaka, M. Kaido, A. Suzuki, N. Yamada, N. Torikai, K. Ishihara and A. Takahara, Friction behavior of high-density poly(2-methacryloyloxyethyl phosphorylcholine) brush in aqueous media, *Soft Matter*, 2007, 3(6), 740–746.
- 20 W. L. Jorgensen, J. Chandrasekhar, J. D. Madura, R. W. Impey and M. L. Klein, Comparison of Simple Potential Functions for Simulating Liquid Water, *J. Chem. Phys.*, 1983, 79(2), 926–935.
- 21 B. W. Li, Z. F. Yuan, P. Zhang, A. Sinclair, P. Jain, K. Wu, C. Tsao, J. Y. Xie, H. C. Hung, X. J. Lin, T. Bai and S. Y. Jiang, Zwitterionic Nanocages Overcome the Efficacy Loss of Biologic Drugs, *Adv. Mater.*, 2018, 30(14), 1705728.
- 22 L. D. Blackman, P. A. Gunatillake, P. Cass and K. E. S. Locock, An introduction to zwitterionic polymer behavior and applications in solution and at surfaces, *Chem. Soc. Rev.*, 2019, 48(3), 757–770.
- 23 Y. N. Chou, F. Sun, H. C. Hung, P. Jain, A. Sinclair, P. Zhang, T. Bai, Y. Chang, T. C. Wen, Q. M. Yu and S. Y. Jiang, Ultralow fouling and high antibody loading zwitterionic hydrogel coatings for sensing and detection in complex media, *Acta Biomater.*, 2016, 40, 31–37.
- 24 W. Yang, T. Bai, L. R. Carr, A. J. Keefe, J. J. Xu, H. Xue, C. A. Irvin, S. F. Chen, J. Wang and S. Y. Jiang, The effect of lightly crosslinked poly(carboxybetaine)hydrogel coating on the performance of sensors in whole blood, *Biomaterials*, 2012, 33(32), 7945–7951.
- 25 J. Liu and J. Zhou, Hydrolysis-controlled protein adsorption and antifouling behaviors of mixed charged self-assembled monolayer: A molecular simulation study, *Acta Biomater.*, 2016, **40**, 23–30.
- 26 Y. Chang, S. H. Shu, Y. J. Shih, C. W. Chu, R. C. Ruaan and W. Y. Chen, Hemocompatible Mixed-Charge Copolymer Brushes of Pseudozwitterionic Surfaces Resistant to Nonspecific Plasma Protein Fouling, *Langmuir*, 2010, 26(5), 3522–3530.
- 27 X. S. Liu, H. Y. Huang, Q. Jin and J. Ji, Mixed Charged Zwitterionic Self-Assembled Monolayers as a Facile Way to Stabilize Large Gold Nanoparticles, *Langmuir*, 2011, 27(9), 5242–5251.
- 28 S. Chen, J. Zheng, L. Li and S. Jiang, Strong resistance of phosphorylcholine self-assembled monolayers to protein adsorption: insights into nonfouling properties of zwitterionic materials, J. Am. Chem. Soc., 2005, 127(41), 14473–14478.
- 29 Y. Chang, S. C. Liao, A. Higuchi, R. C. Ruaan, C. W. Chu and W. Y. Chen, A Highly stable nonbiofouling surface with wellpacked grafted zwitterionic polysulfobetaine for plasma protein repulsion, *Langmuir*, 2008, 24(10), 5453–5458.

- 30 H. Vaisocherova, Z. Zhang, W. Yang, Z. Q. Cao, G. Cheng, A. D. Taylor, M. Piliarik, J. Homola and S. Y. Jiang, Functionalizable surface platform with reduced nonspecific protein adsorption from full blood plasma-Material selection and protein immobilization optimization, *Biosens. Bioelectron.*, 2009, 24(7), 1924–1930.
- 31 M. Ilcikova, J. Tkac and P. Kasak, Switchable Materials Containing Polyzwitterion Moieties, *Polymers*, 2015, 7(11), 2344–2370.
- 32 S. F. Chen, L. Y. Li, C. Zhao and J. Zheng, Surface hydration: Principles and applications toward low-fouling/nonfouling biomaterials, *Polymer*, 2010, **51**(23), 5283–5293.
- 33 Y. Higaki, J. Nishida, A. Takenaka, R. Yoshimatsu, M. Kobayashi and A. Takahara, Versatile inhibition of marine organism settlement by zwitterionic polymer brushes, *Polym. J.*, 2015, 47(12), 811–818.
- 34 W. W. Zhao, Q. Ye, H. Y. Hu, X. L. Wang and F. Zhou, Grafting zwitterionic polymer brushes via electrochemical surface-initiated atomic-transfer radical polymerization for anti-fouling applications, *J. Mater. Chem. B*, 2014, 2(33), 5352–5357.
- 35 H. Chen, J. T. Yang, S. W. Xiao, R. D. Hu, S. M. Bhaway, B. D. Vogt, M. Z. Zhang, Q. Chen, J. Ma, Y. Chang, L. Y. Li and J. Zheng, Salt-responsive polyzwitterionic materials for surface regeneration between switchable fouling and antifouling properties, *Acta Biomater.*, 2016, 40, 62–69.
- 36 J. T. Yang, H. Chen, S. W. Xiao, M. X. Shen, F. Chen, P. Fan, M. Q. Zhong and J. Zheng, Salt-Responsive Zwitterionic Polymer Brushes with Tunable Friction and Antifouling Properties, *Langmuir*, 2015, 31(33), 9125–9133.
- 37 Q. Shao and S. Jiang, Influence of Charged Groups on the Properties of Zwitterionic Moieties: A Molecular Simulation Study, *J. Phys. Chem. B*, 2014, **118**(27), 7630–7637.
- 38 Q. Shao, Y. He, A. D. White and S. Y. Jiang, Difference in Hydration between Carboxybetaine and Sulfobetaine, *J. Phys. Chem. B*, 2010, 114(49), 16625–16631.
- 39 Z. Y. Liu, Q. Jiang, Z. Q. Jin, Z. Y. Sun, W. J. Ma and Y. L. Wang, Understanding the Antifouling Mechanism of Zwitterionic Monomer-Grafted Polyvinylidene Difluoride Membranes: A Comparative Experimental and Molecular Dynamics Simulation Study, ACS Appl. Mater. Interfaces, 2019, 11(15), 14408–14417.
- 40 Y. He, Q. Shao, H.-K. Tsao, S. Chen, W. A. Goddard and S. Jiang, Understanding Three Hydration-Dependent Transitions of Zwitterionic Carboxybetaine Hydrogel by Molecular Dynamics Simulations, *J. Phys. Chem. B*, 2011, 115(40), 11575–11580.
- 41 Y. He, H. K. Tsao and S. Y. Jiang, Improved Mechanical Properties of Zwitterionic Hydrogels with Hydroxyl Groups, *J. Phys. Chem. B*, 2012, **116**(19), 5766–5770.
- 42 J. Zheng, L. Li, S. Chen and S. Jiang, Molecular simulation study of water interactions with oligo (ethylene glycol)terminated alkanethiol self-assembled monolayers, *Langmuir*, 2004, **20**(20), 8931–8938.
- 43 J. Zheng, L. Li, H.-K. Tsao, Y.-J. Sheng, S. Chen and S. Jiang, Strong Repulsive Forces between Protein and Oligo

- (Ethylene Glycol) Self-Assembled Monolayers: A Molecular Simulation Study, *Biophys. J.*, 2005, **89**(1), 158–166.
- 44 J. Zheng, Y. He, S. Chen, L. Li, M. T. Bernards and S. Jiang, Molecular simulation studies of the structure of phosphorylcholine self-assembled monolayers, *J. Chem. Phys.*, 2006, 125(17), 174714.
- 45 Z. Zhang, H. Vaisocherova, G. Cheng, W. Yang, H. Xue and S. Y. Jiang, Nonfouling Behavior of Polycarboxybetaine-Grafted Surfaces: Structural and Environmental Effects, *Biomacromolecules*, 2008, 9(10), 2686–2692.
- 46 J. Zhou, J. Zheng and S. Y. Jiang, Molecular simulation studies of the orientation and conformation of cytochrome *c* adsorbed on self-assembled monolayers, *J. Phys. Chem. B*, 2004, **108**(45), 17418–17424.
- 47 Y. He, J. Hower, S. F. Chen, M. T. Bernards, Y. Chang and S. Y. Jiang, Molecular simulation studies of protein interactions with zwitterionic phosphorylcholine self-assembled monolayers in the presence of water, *Langmuir*, 2008, 24(18), 10358–10364.
- 48 D. L. Cheung and K. H. A. Lau, Atomistic Study of Zwitterionic Peptoid Antifouling Brushes, *Langmuir*, 2019, 35(5), 1483–1494
- 49 Y. Xiang, R. G. Xu and Y. S. Leng, Molecular Simulations of the Hydration Behavior of a Zwitterion Brush Array and Its Antifouling Property in an Aqueous Environment, *Langmuir*, 2018, 34(6), 2245–2257.
- 50 K. Vanommeslaeghe, E. Hatcher, C. Acharya, S. Kundu, S. Zhong, J. Shim, E. Darian, O. Guvench, P. Lopes, I. Vorobyov and A. D. Mackerell, CHARMM general force field: A force field for drug-like molecules compatible with the CHARMM all-atom additive biological force fields, *J. Comput. Chem.*, 2010, 31(4), 671–690.
- 51 J. B. Klauda, R. M. Venable, J. A. Freites, J. W. O'Connor, D. J. Tobias, C. Mondragon-Ramirez, I. Vorobyov, A. D. MacKerell and R. W. Pastor, Update of the CHARMM All-Atom Additive Force Field for Lipids: Validation on Six Lipid Types, J. Phys. Chem. B, 2010, 114(23), 7830–7843.
- 52 I. Vorobyov, V. M. Anisimov, S. Greene, R. M. Venable, A. Moser, R. W. Pastor and A. D. MacKerell, Additive and Classical Drude Polarizable Force Fields for Linear and Cyclic Ethers, J. Chem. Theory Comput., 2007, 3(3), 1120–1133.
- 53 O. Herzberg and J. L. Sussman, Protein Model-Building by the Use of a Constrained-Restrained Least-Squares Procedure, *J. Appl. Crystallogr.*, 1983, **16**, 144–150.
- 54 J. C. Phillips, R. Braun, W. Wang, J. Gumbart, E. Tajkhorshid, E. Villa, C. Chipot, R. D. Skeel, L. Kale and K. Schulten, Scalable molecular dynamics with NAMD, *J. Comput. Chem.*, 2005, 26(16), 1781–1802.
- 55 J. R. Werber, C. O. Osuji and M. Elimelech, Materials for next-generation desalination and water purification membranes, *Nat. Rev. Mater.*, 2016, 1(5), 1–15.
- 56 C. H. Liu, J. Lee, C. Small, J. Ma and M. Elimelech, Comparison of organic fouling resistance of thin-film composite membranes modified by hydrophilic silica nanoparticles and zwitterionic polymer brushes, *J. Membr. Sci.*, 2017, 544, 135–142.

- 57 M. V. Graham, A. P. Mosier, T. R. Kiehl, A. E. Kaloyeros and N. C. Cady, Development of antifouling surfaces to reduce bacterial attachment, *Soft Matter*, 2013, 9(27), 6235–6244.
- 58 J. F. Schumacher, M. L. Carman, T. G. Estes, A. W. Feinberg, L. H. Wilson, M. E. Callow, J. A. Callow, J. A. Finlay and A. B. Brennan, Engineered antifouling microtopographieseffect of feature size, geometry, and roughness on settlement of zoospores of the green alga Ulva, *Biofouling*, 2007, 23(1), 55–62.
- 59 F. Y. Yang, Y. L. Liu, Y. X. Zhang, B. P. Ren, J. X. Xu and J. Zheng, Synthesis and Characterization of Ultralow Fouling Poly(*N*-acryloyl-glycinamide) Brushes, *Langmuir*, 2017, 33(49), 13964–13972.
- 60 S. Herrwerth, W. Eck, S. Reinhardt and M. Grunze, Factors that Determine the Protein Resistance of Oligoether Self-Assembled Monolayers – Internal Hydrophilicity, Terminal Hydrophilicity, and Lateral Packing Density, *J. Am. Chem.* Soc., 2003, 125(31), 9359–9366.
- 61 L. Li, S. Chen, J. Zheng, B. D. Ratner and S. Jiang, Protein adsorption on oligo(ethylene glycol)-terminated alkanethiolate self-assembled monolayers: the molecular basis for nonfouling behavior, *J. Phys. Chem. B*, 2005, **109**(7), 2934–2941.
- 62 Y. Zhang, Y. Liu, B. Ren, D. Zhang, S. Xie, Y. Chang, J. Yang, J. Wu, L. Xu and J. Zheng, Fundamentals and applications of zwitterionic antifouling polymers, *J. Phys. D: Appl. Phys.*, 2019, 52(40), 403001.
- 63 J. A. Mondal, S. Nihonyanagi, S. Yamaguchi and T. Tahara, Three Distinct Water Structures at a Zwitterionic Lipid/Water Interface Revealed by Heterodyne-Detected Vibrational Sum Frequency Generation, *J. Am. Chem. Soc.*, 2012, 134(18), 7842–7850.
- 64 S. Y. Re, W. Nishima, T. Tahara and Y. Sugita, Mosaic of Water Orientation Structures at a Neutral Zwitterionic Lipid/Water Interface Revealed by Molecular Dynamics Simulations (vol. 5, p. 4343, 2014), *J. Phys. Chem. Lett.*, 2015, 6(1), 195.
- 65 D. Lis, E. H. G. Backus, J. Hunger, S. H. Parekh and M. Bonn, Liquid flow along a solid surface reversibly alters interfacial chemistry, *Science*, 2014, 344(6188), 1138–1142.
- 66 J. A. Mondal, S. Nihonyanagi, S. Yamaguchi and T. Tahara, Structure and Orientation of Water at Charged Lipid Monolayer/Water Interfaces Probed by Heterodyne-Detected Vibrational Sum Frequency Generation Spectroscopy, *J. Am. Chem. Soc.*, 2010, 132(31), 10656–10657.
- 67 Q. Shao, L. Mi, X. Han, T. Bai, S. J. Liu, Y. T. Li and S. Y. Jiang, Differences in Cationic and Anionic Charge Densities Dictate Zwitterionic Associations and Stimuli Responses, J. Phys. Chem. B, 2014, 118(24), 6956–6962.
- 68 X. B. Quan, J. Liu and J. Zhou, Multiscale modeling and simulations of protein adsorption: progresses and perspectives, *Curr. Opin. Colloid Interface Sci.*, 2019, 41, 74–85.
- 69 Z. Zhang, M. Zhang, S. F. Chen, T. A. Horbetta, B. D. Ratner and S. Y. Jiang, Blood compatibility of surfaces with

- superlow protein adsorption, *Biomaterials*, 2008, **29**(32), 4285–4291.
- 70 J. Ladd, Z. Zhang, S. Chen, J. C. Hower and S. Jiang, Zwitterionic polymers exhibiting high resistance to non-specific protein adsorption from human serum and plasma, *Biomacromolecules*, 2008, **9**(5), 1357–1361.
- 71 Y. Inoue and K. Ishihara, Reduction of protein adsorption on well-characterized polymer brush layers with varying chemical structures, *Colloids Surf.*, *B*, 2010, **81**(1), 350–357.
- 72 C. R. Emmenegger, E. Brynda, T. Riedel, Z. Sedlakova, M. Houska and A. B. Alles, Interaction of Blood Plasma with Antifouling Surfaces, *Langmuir*, 2009, **25**(11), 6328–6333.